chemistry

MDPI

Article

Trinuclear and Cyclometallated Organometallic Dinuclear Pt-Pyrazolato Complexes: A Combined Experimental and Theoretical Study

Zhichun Shi [1], Fengyu Li [2], Hong Zhao [2], Indranil Chakraborty [1], Zhongfang Chen [2,*] and Raphael G. Raptis [1,*]

[1] Department of Chemistry, Biochemistry and Biomolecular Sciences Institute, Florida International University, Miami, FL 33199, USA
[2] Department of Chemistry, University of Puerto Rico, San Juan, PR 00931, USA
* Correspondence: zhongfang.chen1@upr.edu (Z.C.); rraptis@fiu.edu (R.G.R.)

Abstract: Two differently substituted pyrazole ligands have been investigated with regard to the topology of their Pt complexes: upon deprotonation, two mononuclear 1:2 Pt^{II}-pyrazole complexes—one of the sterically unhindered 4-Me-pzH and one of the bulky 3,5-^{t}Bu-pzH (pzH = pyrazole)—yield the corresponding 1:2 Pt^{II}-pyrazolato species; the former a triangular, trinuclear metallacycle (**1**), and the latter a dinuclear, half-lantern species (**2**) formed via the unprecedented cyclometallation of a butyl group. Stoichiometric oxidation of the colorless Pt^{II}_2 complex produces the deep-blue, metal–metal bonded Pt^{III}_2 analog (**3**) with a rarely encountered unsymmetrical coordination across the Pt-Pt bond. All three complexes have been characterized by single crystal X-ray structure determination, ^{1}H-NMR, IR, and UV-vis-NIR spectroscopic methods. The XPS spectra of the Pt^{II}_2 and Pt^{III}_2 species are also reported. Density functional theory calculations were carried out to investigate the electronic structure, spectroscopic properties, and chemical bonding of the new complexes. The calculated natural population analysis charges and Wiberg bonding indices indicate a weak σ-interaction in the case of **2** and a formal Pt-Pt single bond in **3**.

Keywords: dinuclear complexes; trinuclear complexes; cyclometallation; Pt-pyrazolato complexes; two-electron oxidation; platinum metal–metal bond

Citation: Shi, Z.; Li, F.; Zhao, H.; Chakraborty, I.; Chen, Z.; Raptis, R.G. Trinuclear and Cyclometallated Organometallic Dinuclear Pt-Pyrazolato Complexes: A Combined Experimental and Theoretical Study. *Chemistry* **2023**, *5*, 187–200. https://doi.org/10.3390/chemistry5010016

Academic Editor: Zoi Lada

Received: 19 December 2022
Revised: 23 January 2023
Accepted: 24 January 2023
Published: 29 January 2023

1. Introduction

Metal–metal interactions in multinuclear systems determine the course of their chemical reactions, with implications in industrial and biological catalysis, the construction of functional materials, as well as in the understanding of fundamental chemical principles (e.g., metal–metal bonding). In addition to metal–metal distance and orientation, the role of peripheral ligands is often critical to the reaction outcome, as the steric bulk of groups proximal to the metal allows or prevents the formation of certain products, and the energy of the metal-based frontier orbitals is tuned by the resonance and inductive effects exerted by these groups. Two-electron oxidative addition/reductive elimination reactions across dinuclear or trinuclear late transition metal centers continue to attract considerable interest [1–3]; they can lead to either homovalent or mixed-valent products, depending on the distance between and relative orientation of the redox centers. For example, symmetric two-electron-two-center (2e-2c) oxidative addition across "face-to-face" Au^{I}_2, Pt^{II}_2, or $Au^{I}Pt^{II}Au^{I}$, has led to homovalent products, Au^{II}_2, Pt^{III}_2, and $Au^{II}Pt^{II}Au^{II}$, respectively, containing metal–metal bonds (Scheme 1A–C) [4–7]. On the other hand, when the bridging ligands tilt the coordination planes of the metal centers relative to each other, stepwise 2e-1c reduction of a triangular $Au^{III}_3Cl_6$ complex led to unsymmetrical, mixed-valent $Au^{I}Au^{III}_2Cl_4$ and $Au^{I}_2Au^{III}Cl_2$ products (Scheme 1D). At the same time, a similar photochemical process has been reported for an $Au^{III}_2Cl_4$ generating $Au^{I}Au^{III}Cl_2$ and Au^{I}_2 [8–12]. Mixed-valent 2e-1c oxidative addition products also result in the "face-to-face"

Au^{I}_2 systems in which the Au-centers are widely separated [13]. In the case of a Pt^{II}_2 complex with tilted coordination planes, both two- and four-electron oxidation products, Scheme 1E,F [14], have been obtained, whereas either symmetrical metal–metal bonded, or unsymmetrical two-electron oxidation products have been characterized for the analogous systems, **E** with M = Ru [15], and **F** with Rh and Ir [16,17].

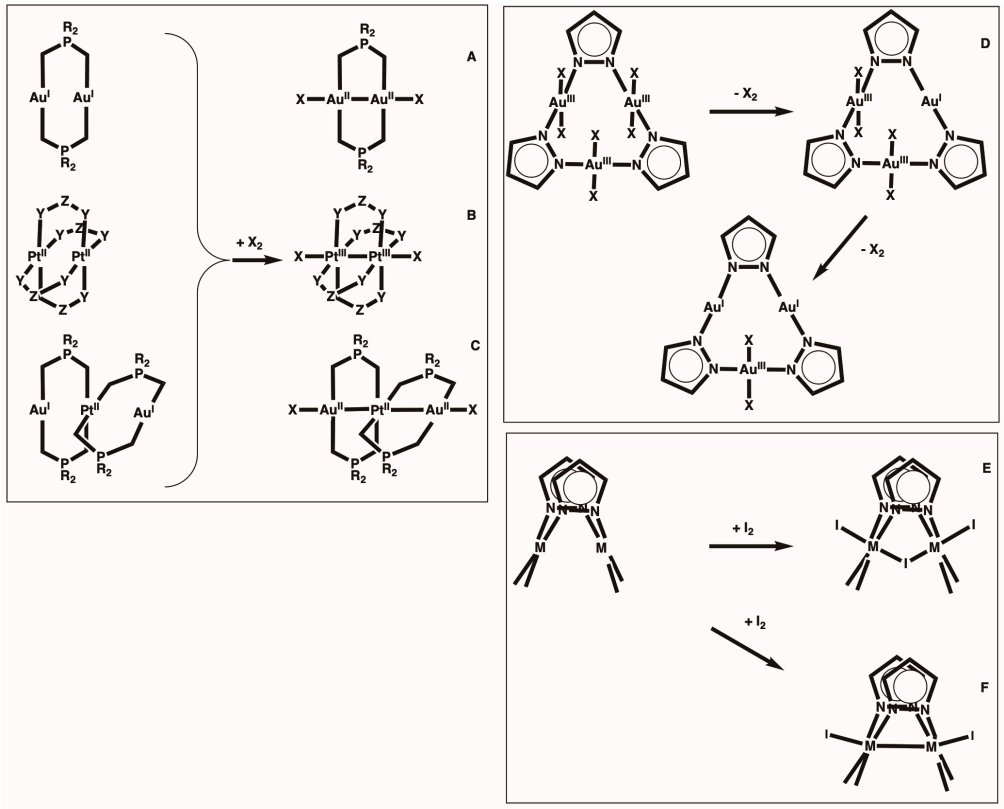

Scheme 1. Oxidative addition/reductive elimination across dinuclear and trinuclear complexes.

In 2006, Umakoshi et al. [18] prepared a delocalized mixed-valent $Pt^{III}_2Pt^{II}$ complex, namely, pyrazolato-bridged platinum cyclic trimer $[Pt_3(\mu\text{-pz})_6Br_2]$, by the two-electron oxidation of its yet not structurally characterized homovalent Pt^{II}_3 precursor. This finding prompted us to reinvestigate dinuclear and trinuclear Pt^{II}-complexes with tilted coordination planes, maintained by bridging pyrazolates [19]. We have employed two pyrazole ligands containing alkyl substituents: one presenting no steric hindrance to the donor N atoms, and one containing bulky tert-butyl groups, the latter forcing a close contact between methyl groups and the N-coordinated metal (Scheme 2). Here, we present the synthesis, structural and spectroscopic characterization, and theoretical studies of three new complexes involving two pyrazole ligands: 4-Me-pzH and 3,5-$^{t}Bu_2$-pzH (pzH = pyrazole), the latter capable of cyclometallating via its ^{t}Bu group. Specifically, the triangular complex $[Pt^{II}(\mu\text{-4-Me-pzH})_2]_3$, **1**, the dinuclear orthometallated complex $[Pt^{II}(\mu\text{-3,5-}^{t}Bu_2\text{-pz})(\kappa^2\text{-N,C-1-H-5-}^{t}\text{Bu-3-CMe}_2\text{CH}_2\text{-pzH})]_2$, **2**, and its two-electron oxidation product $[Pt^{III}_2(\mu\text{-3,5-}^{t}Bu_2\text{-pz})_2(\kappa^2\text{-N,C-1-H-3-CH}_2\text{Me}_2\text{CH}_2\text{-5-}^{t}\text{Bu-pzH})(\kappa^2\text{-N,C-3-CCH}_2\text{Me}_2\text{-5-}^{t}\text{Bu-pz})\text{Cl}]$, **3**, are discussed.

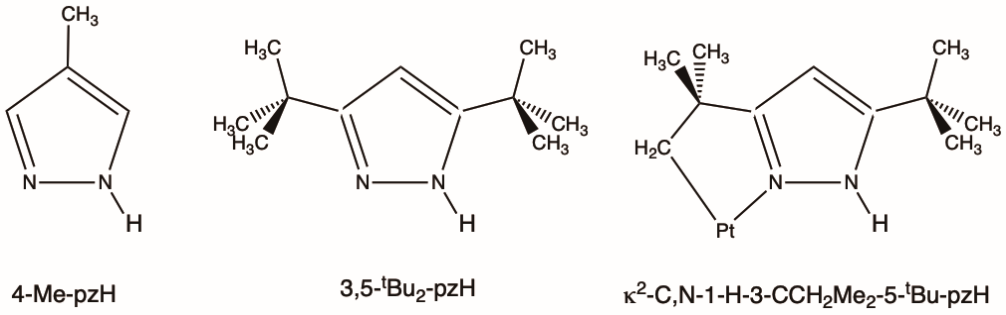

Scheme 2. Two pyrazole ligands employed here and cyclometallation mode.

2. Results and Discussion

2.1. Synthesis and Characterization

Complex **1** was prepared by the same method used for the synthesis of the analogous Pd-complex, $[Pd^{II}(\mu\text{-3-Ph-pz})_2]_3$ [20]. Deprotonation of the pyrazole ligands of *trans*-$[PtCl_2(4\text{-Me-pzH})_2]$ initiated the cyclization of the homoleptic trimer (Scheme 3A). However, the analogous reaction involving 3,5-^{t}Bu$_2$-pzH resulted in the cyclometallated dimer **2** (Scheme 3B). Complex **3** was prepared by the oxidation of **2** by one equivalent of the oxidizing agent (Scheme 3C). The orientation of pyrazolido anion electron donor orbitals favors the formation of triangular species, as long as bulky 3,5-pyrazole substituents do not sterically hinder these species; these tendencies are well documented in the literature [21–23]. In that light, the formation of **1** upon pyrazole deprotonation by a base is unexceptional. In contrast, whereas non-triangular products were expected upon deprotonation of *trans*-$[PtCl_2(3,5\text{-}^t\text{Bu-pzH})_2]$, the cyclometallation of a butyl group is noteworthy: cyclometallation reactions involving activated C-H bonds (typically of aromatic rings or heterocycles) have been reported for 4d and 5d transition metals [24–26], including platinum [27–29]. However, to the best of our knowledge, cyclometallation of a saturated aliphatic group has not been hitherto reported, even though the activation of C-H bonds by platinum is well established in the literature [30,31]. Oxidative addition to a diplatinum(II) complex containing bridging pyrazolates and chelating/orthometallated ligands, similar to the oxidation of **2** to **3** here, has recently been reported also by others [14]. Complexes **1**–**3** were structurally characterized by single-crystal X-ray crystallography. Selected distances and angles pertaining to **1**–**3** are listed in Table 1.

Complex **1** crystallized in the triclinic space group *P*-1 with two molecules of **1** and one-half interstitial acetone solvent molecule per asymmetric unit. The two crystallographically independent molecules of **1** do not differ statistically from each other; both show minor deviation from ideal D_{3h} symmetry (Figure 1). The existence of a single set of resonances for the six pyrazolido ligands in its ^{1}H-NMR spectrum shows that the trimeric structure persists in solution (Figure S1). The Pt centers are in an approximate square planar N_4 environment with the Pt atoms deviating by 0.14–0.15 Å from the best-fit planes of the four N atoms in the direction away from the center of the metallacyclic ring. The intramolecular Pt···Pt distances average 3.0511(6) Å, being statistically indistinguishable from the 3.048(1) Å distance of the corresponding unsubstituted pyrazole complex, $[Pt(\mu\text{-pz})_2]_3$ [32], and quite similar to the average Pd···Pd distances of 3.054(1) Å in $[Pd(\mu\text{-3-Ph-pz})_2]_3$, 3.0471(3) Å in $[Pd(\mu\text{-pz})_2]_3$, and 3.0458(4) Å in $[Pd(\mu\text{-4-Me-pz})_2]_3$ (the ionic radii of Pt^{II} and Pd^{II} differ by 0.06 Å) [20,33,34].

Table 1. Selected experimental and calculated distances (Å) and angles (°) for **1**, **2,** and **3**, calculated data in italics.

	1	**2**	**3**
Pt-Pt	3.0355(5)–3.0758(6) *3.110*, *3.114*, *3.117*	2.9290(5) *3.031*	2.584(3), 2.586(2) *2.640*
Pt-N(μ-pz)	2.006(5)–2.023(5) *2.044–2.047*	2.026(6)–2.157(6) *2.060–2.235*	2.026(7)–2.222(7) *2.068–2.312*
Pt-N(κ^2-pzH)	-	1.961(8) *1.995*, *1.996*	1.973(7)–2.015(7) *2.000*, *2.017*
Pt-C	-	2.048(10), 2.034(10) 2.074, 2.077	2.060(8)–2.078(9) 2.089, 2.100
Pt-Cl	-	-	2.352(3), 2.346(3) *2.434*
Pt-N-N	113.4(4)–116.3(4) *113.3–115.7*	108.9(5)–130.1(6) *110.9–112.6*	101.7(5)–133.7(6) *101.8–111.6*
N-Pt-N (*cis*-pz)	86.6(2)–93.0(2) *81.8–89.2*	89.2(3)–89.3(3) *88.2*	87.6(3)–89.4(3) *88.1–91.1*
N-Pt-N (*trans*)	170.3(2)–172.8(2) *168.2–175.7*	172.2(3)–172.3(3) *175.3*, *175.7*	168.1(3)–174.5(3) *170.2*, *175.0*
N-Pt-C	-	79.3(4), 80.1(4) *79.2*, *79.3*	80.0(3)–81.2(3) *80.5*, *80.6*
Pt-Pt-Cl	-	-	174.72(8), 174.91(7) *173.556*
pz-Pt-Pt-pz	96.9–121.7 (average 110.6) *94.2*, *98.1*, *103.4*	102.6 *105.3*	92.1, 95.9 *92.4*

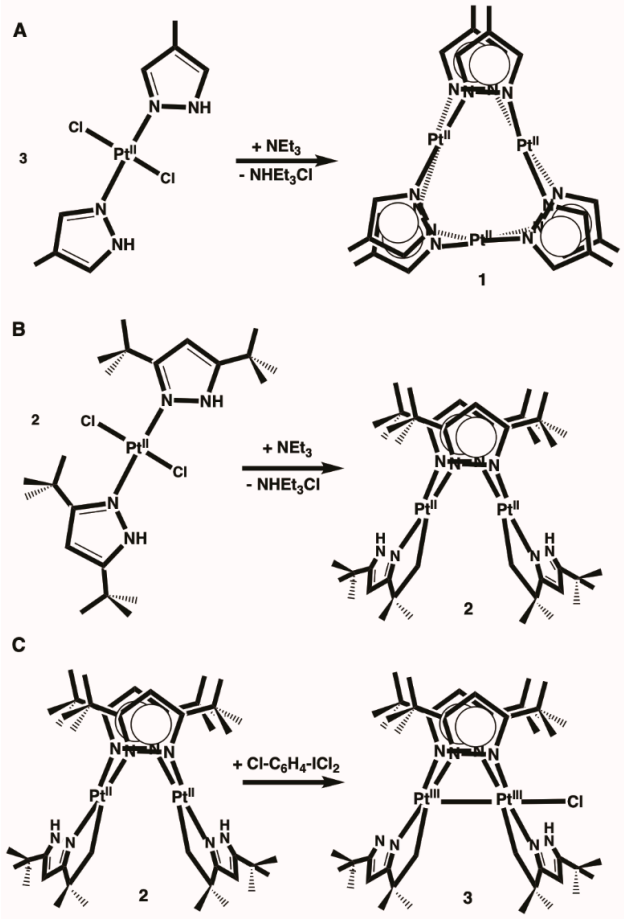

Scheme 3. Synthesis of complexes **1** (**A**), **2** (**B**) and **3** (**C**).

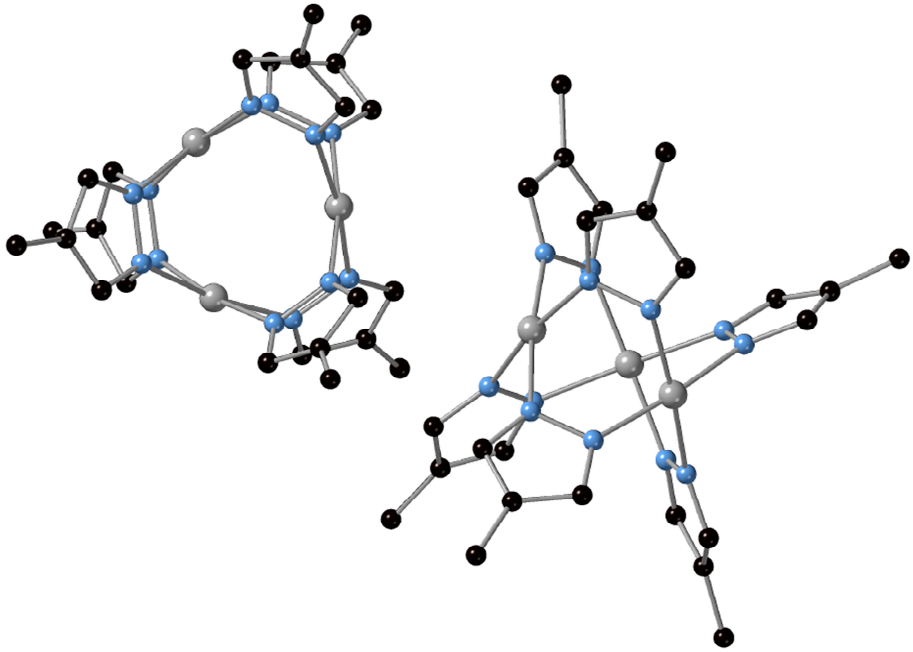

Figure 1. Two ball-and-stick views of the structure of **1**. Color code: C, black; N, blue; Pt, grey. H atoms are not shown for clarity.

Complex **2** crystallized in the chiral orthorhombic space group $P2_12_12_1$ with a whole molecule of C_2 symmetry per asymmetric unit. The structure consists of two Pt atoms, two bridging 3,5-^{t}Bu$_2$-pyrazolato groups, and two chelating cyclometallated 1-H-3-CMe$_2$CH$_2$-5-^{t}Bu-pzH ligands, the latter forming five-membered chelates with each Pt center (Figure 2). The Pt atoms are approximately square-planar with an N_3C-coordination environment. The μ-3,5-^{t}Bu$_2$-pz ligands bridge the metals unsymmetrically, one pyrazole leaning towards one Pt atom (Pt-N = 2.026(7), 2.157(7) Å) and the other leaning the opposite way (Pt-N = 2.151(7), 2.034(7) Å). The solution ^{1}H-NMR spectrum of **2** (Figure 3) is consistent with its solid-state structure. There are four resonances for the cyclometallated butyl-groups: two singlets for the diastereotopic Me groups (1.26 and 0.84 ppm) and two doublets for the diastereotopic, geminal H atoms of CH_2 groups (2.28 and 1.65 ppm); the ^{195}Pt satellites are not observed in this ambient temperature spectrum due to the broadening attributed to the coordination of three quadrupolar N atoms. The Pt···Pt distance of 2.9290(5) Å in **2** is significantly longer than the one determined in a related Pt-(μ-3,5-^{t}Bu$_2$-pz)$_2$-Pt complex, 2.8343(6) Å, containing also 2-(2,4-difluorophenyl)pyridyl chelating ligands [35]. Inspection of a molecular model of **2** shows that the platinum coordination planes are slightly bent to bring the chelating ligands closer to each other than they might have been in an ideal square planar arrangement. In contrast, a much shorter approach between the chelating ligands is found in complex **3** (*vide infra*). Both observations point to Coulombic repulsion between the Pt centers as the more likely explanation for this distortion, rather than the steric repulsion between the chelating cyclometallated ligands.

Complex **3** crystallized in the triclinic space group *P*-1 with two molecules per asymmetric unit, accompanied by four interstitial H_2O molecules at chemically insignificant sites. The structure of **3** retains the basic features of **2**, but with a Pt-Pt separation of 2.584(3) Å and 2.586(2) Å, corresponding to a formal single metal–metal bond and one chloride coordinated trans to it (Figure 4). The C_1 molecular symmetry of **3** is reflected in its ^{1}H-NMR spectrum (Figure 5) showing a doubling of the number of resonances recorded for **2,** in addition to a downfield shift of all resonances, consistent with the increase in its oxidation state. Electroneutrality requires the presence of a crystallographically invisible proton on one of the two non-coordinated N atoms of **3**; this proton is evident in the ^{1}H-NMR by a broad resonance at 8.63 ppm whose integrated area corresponds to one H atom per molecule of **3**. The absence of paramagnetically shifted resonances in **3** is

consistent with its Pt^{III}_2 assignment and the presence of a Pt-Pt bond of 2.585 Å. The latter bond length is shorter than the corresponding unsupported bonds of 2.694(1) Å, 2.6964(5) Å, and 2.726 Å [36–38] reported earlier, but within the range of several ligand-bridged diplatinum(III) species [39,40]. The Pt^{III}_2 oxidation state assignment is further supported by a comparison of the 4f electron binding energies of **2** and **3** determined by X-ray photoelectron spectroscopy (Figure S2) and a comparison with the corresponding binding energies of Pt^{IV} species reported in the literature (Table 2). The experimental XPS peaks of **3** are deconvoluted into two equal components, attributed to its two distinct Pt sites, both with higher binding energies than those of **2** and lower than the literature values for Pt^{IV} compounds [41,42].

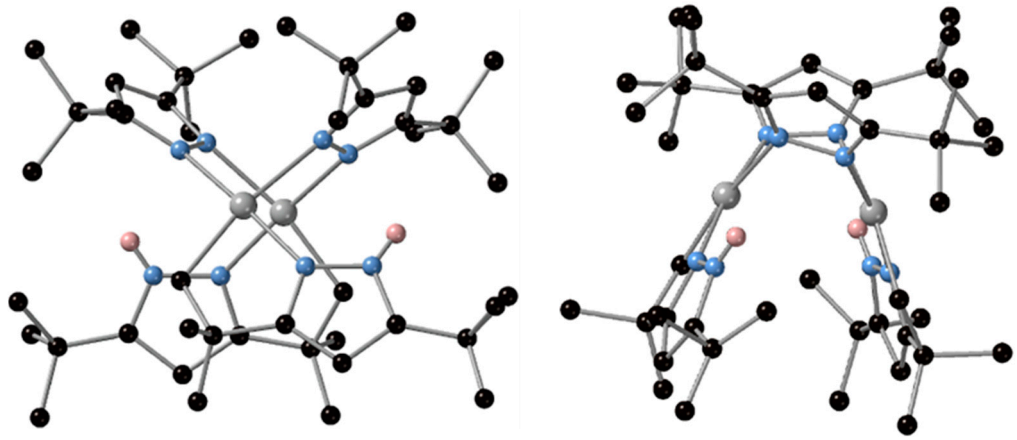

Figure 2. Two ball-and-stick views of the structure of **2**. Color code: C, black; H, pink; N, blue; Pt, grey. H atoms, except for two N-H, are not shown for clarity.

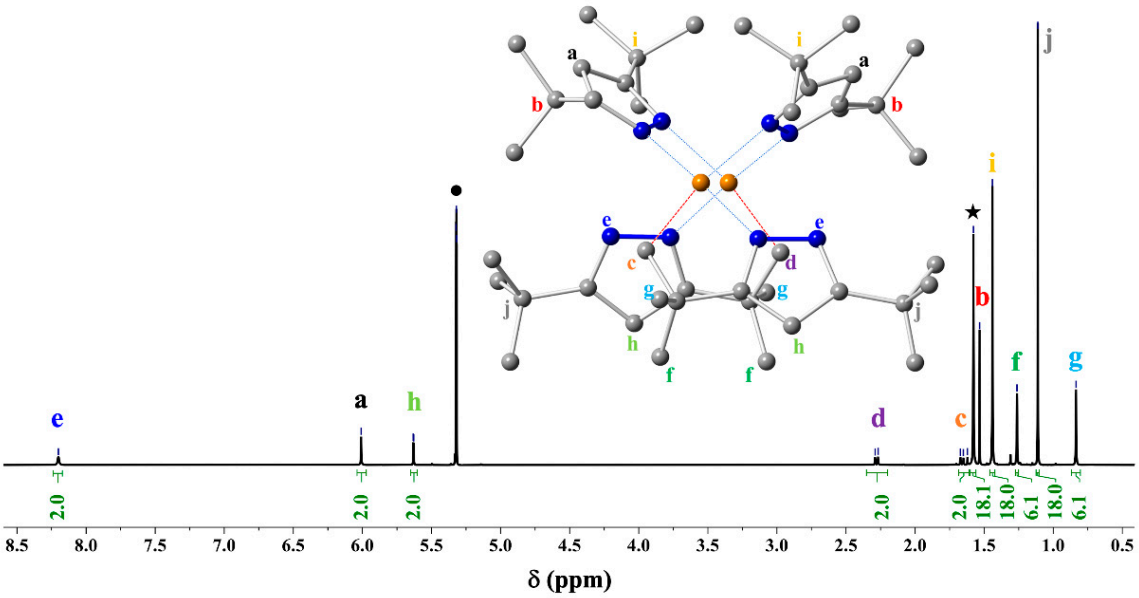

Figure 3. ^{1}H NMR of **2** in CD_2Cl_2 at 293 K. Solvent peaks are identified by solid dot ($CHDCl_2$) or star (H_2O). Peak integrations in green. Protons, except N-H, are omitted for clarity. Inset: Ball-and-stick diagram of **2** with proton labels.

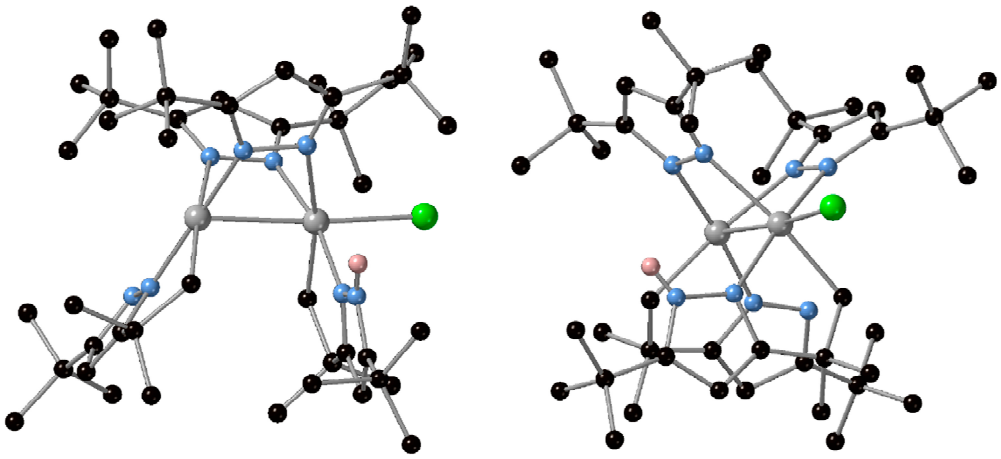

Figure 4. Two ball-and-stick views of the structure of **3**. Color code: C, black; H, pink; N, blue; Pt, grey; Cl, green. H atoms, except for N-H, are not shown for clarity.

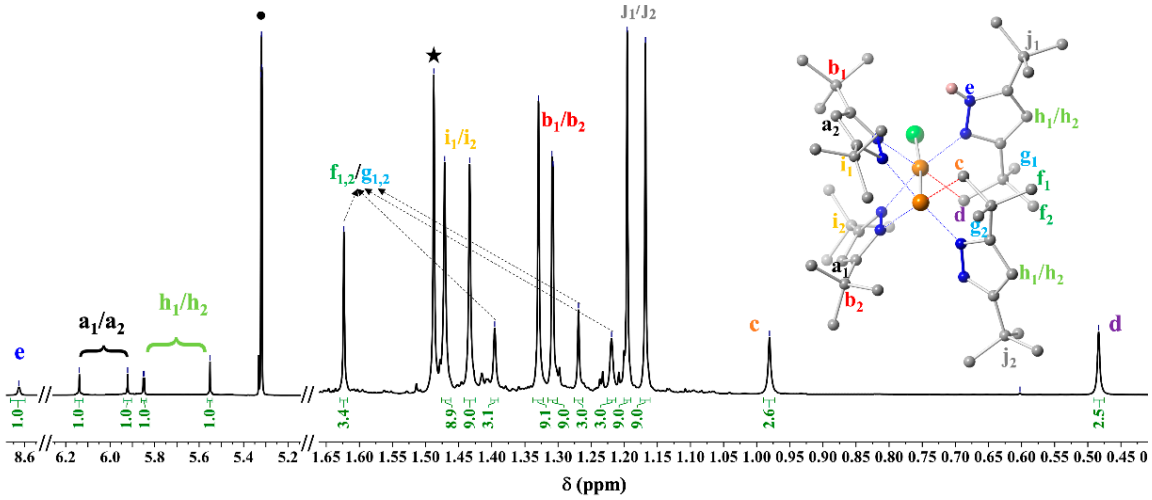

Figure 5. ^{1}H NMR of **3** in CD_2Cl_2 at 293 K. Solvent peaks are identified by solid dot ($CHDCl_2$) or star (H_2O). Peak integrations in green. Protons, except N-H, are omitted for clarity. Inset: Ball-and-stick diagram of **3** with proton labels.

Table 2. Electron binding energies for **2**, **3,** and two Pt^{IV} compounds.

Compound	$4f_{7/2}$ (eV)	$4f_{5/2}$ (eV)
2	72.6	75.4
3 (PtN_3CCl)	73.1	76.4
3 (PtN_3C)	74.4	77.7
H_2PtCl_6	75.2 [a]	78.6 [a]
[Pt(oxa)$(OH)_2$(dachex)]	75.6 [a]	79.0 [a]

[a] Data from references [41,42].

A structural comparison of **2** and **3** shows that the shortening of the separation between the two metal centers, brought about by the formation of a Pt-Pt bond, is accompanied by a decrease in the dihedral angles formed between the μ-3,5-$^{t}Bu_2$-pz ligands from 102.5° in **2** to 92.1° and 95.9° in **3**. The pyrazole–pyrazole dihedral angles of both **2** and **3** are more acute than the 110.6° (average) angle of the less sterically hindered **1**. This agrees with the earlier observation that the Pt-Pt separation in a series of Pt-(μ-3,5-R_2-pz)$_2$-Pt complexes increases as the steric bulk of the bridging ligands decreases [35]. The electronic spectra of **1**, **2,** and **3** each contain an intense UV band with λ_{max} at 225–230 nm, attributed to π-π*

transitions. However, compound **3** shows five additional bands spanning the UV to NIR range—361 nm, 531 nm, 587 nm, 761 nm, and 818 nm—attributed to states arising from the Pt-Pt bonding manifold (Figure S4). To further probe the bonding in the complexes, density functional theory (DFT) calculations were carried out.

2.2. Computational Studies

The optimized geometries agree with the corresponding experimental X-ray structural values of **1–3** (Table 2). We ascertained that all optimized geometries exhibited no imaginary frequency. The computed bond length is slightly larger (0.02–0.10 Å) than the experimental data, since the molecules were optimized in the gas phase, and there is no interaction with other complex units as in the crystalline phase.

The DFT-simulated infrared spectra (IR) of the three complexes are shown in Figure S3. The infrared (IR) spectrum of complex **1** is clearly distinguished from those of **2** and **3** due to its different structure. Complexes **2** and **3** have approximately the same IR distribution, as they share similar structural features, except for the additional Cl atom in **3**. A calculated mode of 286.6 cm^{-1}, assigned to Pt-Cl stretching in complex **3**, falls outside the experimentally accessible spectral window. No Pt-Pt interaction mode is identified in complex **2**.

The HOMO-LUMO gaps of the Pt complexes computed by BP86 functional are 0.26, 2.74, and 0.94 eV for **1**, **2,** and **3**, respectively. The frontier molecular orbitals of Pt complex **1**, **2**, and **3** are presented in Figure S5. The d_z2 orbitals of Pt atoms dominate the HOMO of complexes **1** and **2**, and Pt d-orbitals also contribute to their HOMO-1, HOMO-2, LUMO, LUMO+1, and LUMO+2. However, for complex **3**, the d_z2 orbitals of Pt and the p orbital of Cl contribute to the LUMO, the π orbital of pyrazole, d orbital of Pt, and p orbital of Cl contribute to the HOMO, and the π orbital of pyrazole mainly contribute to the HOMO-1, HOMO-1, LUMO+1, and LUMO+2. The LUMO of **2** consists of d_{xy} and d_{xz} of Pt atoms, and the overlap of the two orbitals exhibit a σ-bonding character, resulting in a shorter Pt-Pt distance than **1**.

To help understand the bonding characteristics of these complexes, we calculated the natural population analysis (NPA) charges and the Wiberg bond index (WBI) based on natural bonding orbital (NBO) computations at the BP86/6–31G*~dz level of theory. The Pt atoms are positively charged (ca. 0.43, 0.44, and 0.47 |e| in **1**; 0.35 |e| in **2**; and 0.46, 0.56 |e| in **3**), and the N/C/Cl atoms are negatively charged (for details see Table S4). Correspondingly, the natural electron configurations for Pt, N, Cl, and C (bonded to Pt) atoms are listed in Table S4. Pt atoms transfer considerable charge (ca. ~0.5 e) to the N/C/Cl atoms of all three complexes. The computed WBIs (Table S5) for Pt-Pt in **3** (0.28) are strikingly larger than that in **1** (0.08~0.09) and **2** (0.06), contributing to the shorter Pt-Pt distance in **3**; the WBIs for Pt-N are comparable in the three complexes. These indicate that partial bonds form between Pt atoms and their surrounding Pt/N/C/Cl atoms, along with a weak σ-interaction in **2** and a formal Pt-Pt single bond in **3**.

QTAIM topological analysis of the electronic density [43–45] gave further details of the bonding in the three Pt complexes. For simplicity, we substituted the methyl groups by H, and the BP86/6–31G*~dz optimized results provide almost the same structural parameters as the initial configurations. Figure 6 depicts the simplified complexes' molecular graphs (at BP86/6–31G*~dz) representing Pt-Pt/Pt-N/Pt-C interactions. The bond critical points (BCPs) between Pt atoms for all three complexes lead to 3, 0, and 1 bond paths for the **1**, **2**, and **3**, respectively. The larger 0.05 au ρ_{bcp} electron densities at the Pt-Pt bond critical points (BCPs) for complex **3** compared to the value of 0.02 au for complex **1** suggest stronger bonds, consistent with the shorter Pt-Pt distance in complex **3**. Note that there is no BCP between Pt and Pt in complex **2**, leading to the longer Pt-Pt distance compared to complex **3**. In addition, the low electron densities ρ_{bcp} (0.11~0.13 au, 0.09~0.14 au, and 0.08~0.14 au in **1**, **2,** and **3**, respectively), as well as negative Laplacian $\nabla^2\rho_{bcp}$ (−0.11~−0.14 au, −0.05~−0.15 au, and −0.04~−0.13 au for **1**, **2** and **3**, respectively), located at the Pt-N/Pt-C/Pt-Cl BCPs, indicate ionic interactions and limited contributions to the total stability.

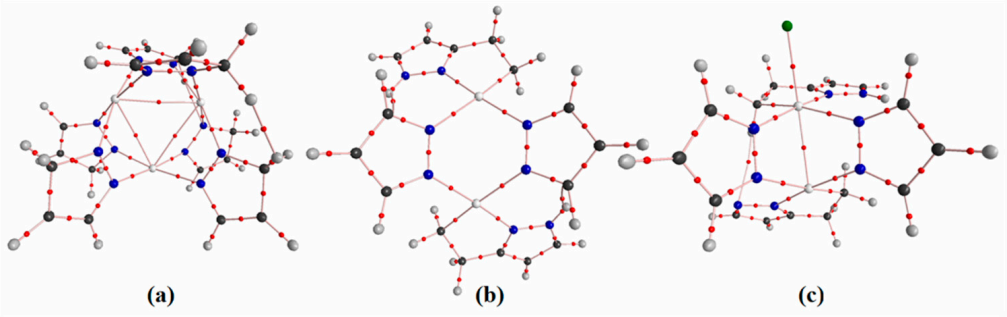

Figure 6. Molecular graphs of the simplified (**a**) **1** (**b**) **2**, and (**c**) **3** configurations. Ring and cage BCPs are omitted for clarity. The red spheres at the center of the interatomic bond lines denote the bond critical points (BCP).

3. Materials, Methods, and Computational Details

Commercial reagents—K_2PtCl_4, 4-Me-pyrazole, pivaloylmethane, and hydrazine—were used as received. 3,5-Di-tert-butyl-pyrazole (3,5-^{t}Bu$_2$-pzH) was prepared by refluxing equivalent amounts of dipivaloylmethane and hydrazine in 95% EtOH. *Trans*-[$PtCl_2$(4-Me-pzH)$_2$] and *trans*-[$PtCl_2$(3,5-^{t}Bu$_2$-pzH)$_2$] were prepared quantitatively by stoichiometric addition of two equivalents of 4-Me-pzH, or 3,5-^{t}Bu$_2$-pzH, to K_2PtCl_4 in MeOH/H_2O and characterized by X-ray structure determination (Tables S1–S3). Solid p-Cl-C_6H_4-ICl_2 was prepared by bubbling gaseous Cl_2 through a solution of p-Cl-C_6H_4-I in toluene and collecting the product by filtration after washing with toluene and diethylether (Caution! The reaction should be carried out under a fume hood with a solution of a base trapping excess Cl_2). Solvents were purified by standard methods [46]. ^{1}H-NMR spectra were recorded with a Bruker Avance DPX-400 spectrometer. ^{13}C-NMR resonances could not be safely distinguished from baseline noise due to solubility limitations. The electronic spectra of the complexes in solution were recorded on a Varian CARY 500 spectrophotometer in the 40,000–4000 cm^{-1} (250–2500 nm) range. Elemental analyses were performed by Galbraith Laboratories, Inc., Knoxville, TN.

[Pt^{II}(μ-4-Me-pz)$_2$]$_3$, 1: To a CH_3CN solution (50 mL) of *trans*-[$PtCl_2$(4-Me-pzH)$_2$] (230 mg, 0.53 mmol) was added Et_3N (162 mg, 1.60 mmol), and the solution was refluxed for 8 h. Yellow solid precipitated and was removed by filtration while the solution was still hot. The colorless filtrate was concentrated under air, yielding a white microcrystalline solid, which was collected and air-dried; Yield, 55 mg (29%). Colorless crystals of **1**, suitable for X-ray analysis, were grown from MeOH/CH_3COCH_3. Anal. Calcd. for $C_{24}N_{12}H_{30}Pt_3$: C, 26.89; H, 2.82; N, 15.68%. Found: C, 27.14; H, 2.79; N, 15.93%. ^{1}H-NMR (CD_3OD, δ, ppm, 400 MHz, 293 K): 7.88 (12H, s, pz-H^{3,5}), 2.06 (18H, s, CH_3). UV-vis-NIR (CH_2Cl_2, λ_{max}[nm]/ε[M^{-1}cm^{-1}]): 229/14200.

[Pt^{II}(μ-3,5-^{t}Bu$_2$-pz)(κ^2-N,C-1-H-5-^{t}Bu-3-CMe$_2$CH$_2$-pzH)]$_2$, 2: To a $CHCl_3$ solution (50 mL) of *trans*-[$PtCl_2$(3,5-^{t}Bu$_2$-pzH)$_2$] (313 mg, 0.5 mmol) was added Et_3N (302 mg, 3.0 mmol) and the solution was refluxed for 10 h. After filtration, the filtrate was concentrated under the air. Colorless crystals of **2**, suitable for X-ray analysis, were collected and washed with MeOH; Yield, 127 mg (46%). Anal. Calcd. for $C_{44}N_8H_{76}Pt_2$: C, 47.73; H, 6.93; N, 10.12%. Found: C, 47.85; H, 6.55; N, 10.21%. ^{1}H-NMR (CD_2Cl_2, δ, ppm, 400 MHz, 293 K): 8.20 (2H, s, N-H), 6.01(2H, s, μ-pz-H^4), 5.63 (2H, κ^2-pz-H^4), 2.28 (2H, d, $^2J_{H-H}$ = 8.8 Hz, Pt-CH_2), 1.65 (2H, d, $^2J_{H-H}$ = 20.0 Hz, C(CH_2)), 1.58 (18H, s, C(CH_3)$_3$), 1.44 (18H, ^{t}Bu$_{μ-pz}$), 1.26 (6H, C(CH_2)$_2$), 1.11 (18H, ^{t}Bu$_{κ-pzH}$), 0.84 (6H, C(CH_2)$_2$). UV-vis-NIR (CH_2Cl_2, λ_{max}[nm]/ε[M^{-1}cm^{-1}]): 225/16,500.

[Pt^{III}$_2$(μ-3,5-^{t}Bu$_2$-pz)$_2$(κ^2-N,C-1-H-3-CMe$_2$CH$_2$-5-^{t}Bu-pzH)(κ^2-N,C-3-CMe$_2$CH$_2$-5-^{t}Bu-pz)Cl], 3: To a colorless CH_2Cl_2 solution of **2** (110.7 mg, 0.1 mmol) was added p-Cl-C_6H_4-ICl_2 (236.9 mg, 0.2 mmol). The solution turned black immediately, and the reaction was allowed for 0.5 h, followed by filtration. Single crystals of **3** were grown by slow diethyl ether vapor diffusion into the filtrate. Yield, 100.35 mg (90%). ^{1}H-NMR (CD_2Cl_2, δ, ppm):

8.63 (1H, s, N-H, $w_{1/2}$ = 4.32 Hz), 6.14 (1H, s, μ-pz-H^4), 5.92 (1H, s, μ-pz-H^4), 5.85 (1H, d, pz-H^4_{pzH}, $^4J_{H\text{-}H(N)}$ = 2.2 Hz), 5.55 (1H, s, pz-H^4_{pz}), 1.62 (3H, s, Pt-CCH_3), 1.47 (9H, s, ^{t}Bu), 1.43 (9H, s, ^{t}Bu), 1.40 (3H, s, Pt-CCH_3), 1.33 (9H, s, $C(CH_3)_3$), 1.31 (9H, s, $C(CH_3)_3$), 1.27 (3H, s, Pt-CCH_3), 1.22 (9H, s, $C(CH_3)_3$), 1.17 (9H, s, $C(CH_3)_3$), 0.98 (2H, s, Pt-CH_2), 0.48 (2H, s, Pt-CH_2). UV-vis-NIR (CH_2Cl_2, λ_{max}[nm]/ε[$M^{-1}cm^{-1}$]): 229/32,700, 361/6300, 531/600, 587/1450, 761/1440, 818/450.

X-ray diffraction data were collected with a Bruker AXS SMART 1K CCD diffractometer [47], using graphite-monochromated Mo-Kα radiation at ambient temperature from single crystals mounted atop glass fibers at random orientation. Data were corrected for Lorentz and polarization effects [48]. The structures were solved employing the SHELXTL-direct methods program and refined by full-matrix least-squares on F^2 [49]. Crystallographic details for **1**, **2**, and **3** are summarized in Table 3.

Table 3. Crystallographic data for **1**, **2**, and **3**.

	1·0.5CH_3COCH_3	**2**	**3·2H_2O**
Formula	$C_{25.5}H_{33}N_{12}O_{0.5}Pt_3$	$C_{44}H_{76}N_8Pt_2$	$C_{44}H_{41}ClN_8O_2Pt_2$
Crystal size, mm^3	0.08 × 0.06 × 0.05	0.40 × 0.30 × 0.20	0.22 × 0.18 × 0.10
fw	1100.91	1107.30	1173.75
Space group	*P*-1 (No. 2)	$P2_12_12_1$ (No. 19)	*P*-1 (No. 2)
a, Å	13.734(3)	12.373(1)	11.643(9)
b, Å	13.837(2)	18.696(2)	21.040(2)
c, Å	17.734(3)	21.343(2)	23.064(13)
α, °	74.55(1)	90	64.77(7)
β, °	81.87(1)	90	83.98(6)
γ, °	74.81(1)	90	82.48(8)
V, $Å^3$	3125.5(9)	4937.2(8)	5059(7)
Z	2	4	4
T, K	298(2)	298(2)	298(2)
ρ_{calcd}, g cm^{-3}	2.34	1.49	1.54
reflctns collected/$2\theta_{max}$	11,453/51.00	29,004/52.00	28,262/50.00
Unique reflctns/I > 2σ(I)	12,088/10,030	9589/8743	17,509/13,447
No. of params/restraints	753/0	513/46	1071/0
μ(Mo Kα), mm^{-1}	13.433	5.696	5.617
F(000)	2032	2208	2336
R1 [a]/All data	0.0285/0.0389	0.0311/0.0402	0.0471/0.0773
wR2 [b] (I > 2σ(I))	0.0663	0.0698	0.1245
Goodness of fit [c]	1.057	1.184	1.039

[a] $I > 2\sigma(I)$. $R1 = \Sigma||F_o| - |F_c||/\Sigma|F_o|$. [b] $wR2 = [\Sigma[w(F_o^2 - F_c^2)^2]/\Sigma[w(F_o^2)^2]]^{1/2}$, where $w = 1/\sigma^2(F_o^2) + (aP)^2 + bP$, $P = (F_o^2 + 2F_c^2)/3$. [c] $GoF = [\Sigma[w(F_o^2 - F_c^2)^2]/(n-p)]^{1/2}$.

The Gaussian 09 software package was employed throughout our density functional theory (DFT) computations [50]. Full geometry optimizations for the three complexes were carried out using the BP86 functional [51,52]. The 6–31G* basis set for C, N, H, and Cl atoms and a double-ζ basis set (LanL2DZ) with the effective core potential (ECP) for Pt (denoted here by 6–31G*∼dz) were used. All the optimized geometries were characterized as true local minima by harmonic vibrational frequency analysis at the same theoretical level. Atomic charges were based on the Natural Population Analysis (NPA) of Weinhold et al. [53]. To gain more insights into the chemical bonding, we performed a quantum theory of atoms in molecules (QTAIM) [43–45] study, using the all-electron basis set (6–31G* for C, N, Cl, and H; double zeta plus polarization function basis set, Douglas–Kroll–Hess for Pt) [54] by AIM2000 software [55]. Natural bond orbital NBO population analysis was used to describe the details of chemical bonding in the systems studied.

4. Conclusions

Differences in the steric bulk of peripheral substituents between the two pyrazoles employed here determine the topology of the resulting pyrazolato products, yielding upon

deprotonation the new trinuclear homoleptic complex **1**, or the dinuclear **2**. Platinum(II) complexes involving less sterically crowded, 3,5-Me2-pzH and 3-^{t}Bu-pzH ligands have been employed in the stepwise construction of multinuclear heterometallic complexes via straightforward coordination chemistry [56,57]. In contrast, the bulky 3,5-$^{t}Bu_2$ groups employed here apparently prevent the formation of a trimeric ring, leaving the Pt center coordinatively unsaturated. The latter satisfies the four-coordination requirement of Pt^{II} via the unprecedented cyclometallation of a tert-butyl group (C-H BDE of ~100 kcal/mol), suggesting possible further applications of 3,5-$^{t}Bu_2$-pzH in C-H activation chemistry and catalysis. Dinuclear half-lantern Pt^{II} complexes, with even longer Pt . . . Pt separation than **2**, have been studied in detail with regard to their tunable visible luminescence [35,58–63]. In contrast, compound **2** does not luminesce; this is tentatively attributed to the proximity to Pt atoms of the (cyclometallated) C-H group, whose vibrational modes can quench the excited state. The facile oxidative addition of complex **2** to a $Pt^{III}{}_2$ product was expected. However, the unsymmetrical addition of chloride across the Pt-Pt single bond of **3**, while not unprecedented [14], is a rare example of this type of reactivity. The chemistry of five-coordinate (i.e., coordinatively unsaturated) Pt^{III} centers, such as one of the two Pt centers of **3**, remains unexplored, to date.

Supplementary Materials: The following supporting information can be downloaded at: https://www.mdpi.com/article/10.3390/chemistry5010016/s1, Figure S1: ^{1}H NMR of **1**; Figure S2: XPS spectra of **2** and **3**; Figure S3: Calculated and observed FT-IR spectra of **1**, **2** and **3**; Figure S4: UV-vis-NIR spectra of **1**, **2** and **3**; Figure S5: Important molecular orbitals of **1**, **2** and **3**; Figure S6: ORTEP diagram of **1**; Figure S7: ORTEP diagram of **2**; Figure S8: ORTEP diagram of **3**; Figure S9: ORTEP diagram of *trans*-[$PtCl_2$(3,5-$^{t}Bu_2$-pzH)$_2$]; Figure S10: ORTEP diagram of *trans*-[$PtCl_2$(4-Me-pzH)$_2$]; Table S1: Crystallographic data for *trans*-[$PtCl_2$(3,5-$^{t}Bu_2$-pzH)$_2$] and *trans*-[$PtCl_2$(4-Me-pzH)$_2$]; Table S2: Selected bond lengths and angles for [$PtCl_2$(3,5-$^{t}Bu_2$-pzH)$_2$]; Table S3: Selected bond lengths(Å) and angles(°) for [$PtCl_2$(4-Me-pzH)$_2$]; Table S4: Computed NBA charges and natural electron configurations of the selected atoms **1**, 2 and **3**; Table S5: Computed WBI Pt-Pt/Pt-N/Pt-C/Pt-Cl bonds in the three simplified Pt complexes; Table S6: Selected bond lengths and bond angles for **1**; Table S7: Selected bond lengths and bond angles for **2**; Table S8: Selected bond lengths and bond angles for **3**; Crystallographic data are available free of charge via the Internet at CCDC numbers: 2221215 (**1**) 2221216 (**2**), 2221217 (**3**), 2221218 ([$PtCl_2$(3,5-$^{t}Bu_2$-pzH)$_2$]), and 2221219 ([$PtCl_2$(4-Me-pzH)$_2$]).

Author Contributions: Conceptualization, R.G.R.; methodology, H.Z. and F.L.; formal analysis, Z.S., H.Z. and I.C.; investigation, Z.S., F.L. and H.Z.; resources, R.G.R. and Z.C.; writing—original draft preparation, Z.S., F.L. and R.G.R.; writing—review and editing, R.G.R. and Z.C.; visualization, Z.S., F.L. and I.C.; supervision, R.G.R. and Z.C.; project administration, R.G.R.; funding acquisition, R.G.R. and Z.C. All authors have read and agreed to the published version of the manuscript.

Funding: This material is based upon work supported by the National Science Foundation under Grant No. NSF-DMR-2122078. Work in UPR has been supported by the National Science Foundation under Grant No. NSF-EPS-1010094.

Data Availability Statement: Not applicable.

Acknowledgments: R.G.R. is grateful to Johnson Matthey Co. for a generous gift of potassium tetrachloroplatinate.

Conflicts of Interest: The authors declare no conflict of interest.

References

1. Fackler, J.P., Jr. Metal-metal bond formation in the oxidative addition to dinuclear gold(I) species. Implications from dinuclear and trinuclear gold chemistry for the oxidative addition process generally. *Polyhedron* **1997**, *16*, 1–17. [CrossRef]
2. Fackler, J.P., Jr. Forty-Five Years of Chemical Discovery Including a Golden Quarter-Century. *Inorg. Chem.* **2002**, *41*, 6959–6972. [CrossRef] [PubMed]
3. Schenck, T.G.; Milne, C.R.C.; Sawyer, J.F.; Bosnich, B. Bimetallic reactivity. Oxidative-addition and reductive-elimination reactions of rhodium and iridium bimetallic complexes. *Inorg. Chem.* **1999**, *24*, 2338–2344. [CrossRef]
4. Laguna, A.; Laguna, M. Coordination chemistry of gold(II) complexes. *Coord. Chem. Rev.* **1999**, *193–195*, 837–856. [CrossRef]

5. Cotton, F.A.; Murillo, C.A.; Walton, R.A. (Eds.) *Multiple Bonds between Metal Atoms*, 3rd ed.; Springer Science and Business Media, Inc.: New York, NY, USA, 2005; Chapter 14; pp. 636–661.
6. Matsumoto, K.; Ochiai, M. Organometallic chemistry of platinum-blue derived platinum III dinuclear complexes. *Coord. Chem. Rev.* **2002**, *231*, 229–238. [CrossRef]
7. Murray, H.H., III; Briggs, D.A.; Garzón, G.; Raptis, R.G.; Porter, L.C.; Fackler, J.P., Jr. Structural Characterization of a Linear [Au···Pt···Au] Complex, $Au_2Pt(CH_2P(S)Ph_2)_4$, and its Oxidized Linear Metal-Metal Bonded [Au-Pt-Au] Product, $Au_2Pt(CH_2P(S)Ph_2)_4Cl_2$. *Organometallics* **1987**, *6*, 1992–1995. [CrossRef]
8. Yang, G.; Matínez, J.R.; Raptis, R.G. Dinuclear gold(III) pyrazolato complexes—Synthesis, structural characterization and transformation to their trinuclear gold(I) and gold(I/III) analogues. *Inorg. Chim. Acta* **2009**, *362*, 1546–1552. [CrossRef]
9. Yang, G.; Raptis, R.G. Oxidation of gold(I) pyrazolates by aqua regia. X-Ray crystal structures of the first examples of trinuclear Au^{III}_3 and $Au^{I}Au^{III}_2$ pyrazolato complexes. *J. Chem. Soc. Dalton Trans.* **2002**, *21*, 3936–3938. [CrossRef]
10. Raptis, R.G.; Fackler, J.P., Jr. The synthesis and crystal structure of a mixed-valence, digold(I)/gold(III), pyrazolato complex stable in aqua regia. The x-ray photoelectron study of homo- and heterovalent gold-pyrazolato trimers. *Inorg. Chem.* **1990**, *29*, 5003–5006. [CrossRef]
11. Raptis, R.G.; Murray, H.H.; Fackler, J.P., Jr. The structure of [Au-μ-{3,5-$(C_6H_5)_2C_3HN_2$}]$_3Cl_2$: A trinuclear mixed-valence gold pyrazolate complex. *Acta Crystallogr.* **1988**, *C44*, 970–973. [CrossRef]
12. Teets, T.S.; Nocera, D.G. Halogen Photoreductive Elimination from Gold(III) Centers. *J. Am. Chem. Soc.* **2009**, *131*, 7411–7420. [CrossRef] [PubMed]
13. Irwin, M.J.; Rendina, L.M.; Puddephatt, R.J. A strategy for synthesis of large gold rings. *Chem. Commun.* **1996**, *11*, 1281–1282. [CrossRef]
14. Arnal, L.; Escudero, D.; Fuertes, S.; Martin, A.; Sicilia, V. High-Valent Pyrazolate-Bridged Platinum Complexes: A Joint Experimental and Theoretical Study. *Inorg. Chem.* **2022**, *61*, 12559–12569. [CrossRef] [PubMed]
15. Song, Y.-H.; Chi, Y.; Chen, Y.-L.; Liu, C.-S.; Ching, W.-L.; Carty, A.J.; Peng, S.-M.; Lee, G.-H. A Study of Unsaturated Pyrazolate-Bridged Diruthenium Carbonyl Complexes. *Organometallics* **2002**, *21*, 4735–4742. [CrossRef]
16. Tejel, C.; Ciriano, M.A.; Lopez, J.A.; Lahoz, F.J.; Oro, L.A. New Perspective on the Formation and Reactivity of Metal−Metal-Bonded Dinuclear Rhodium and Iridium Complexes. *Organometallics* **1997**, *16*, 4718–4727. [CrossRef]
17. Coleman, A.W.; Eadie, D.T.; Stobart, S.R.; Zaworotko, M.J.; Atwood, J.L. Pyrazolyl-bridged iridium dimers. 2. Contrasting modes of two-center oxidative addition to a bimetallic system and reductive access to the starting complex: Three key diiridium structures representing short nonbonding and long and short bonding metal-metal interactions. *J. Am. Chem. Soc.* **1982**, *104*, 922–923.
18. Umakoshi, K.; Kojima, T.; Kim, Y.H.; Onishi, M.; Nakao, Y.; Sasaki, S. Deep Blue Mixed-Valent $Pt^{III}Pt^{III}Pt^{II}$ Complex [Pt_3Br_2(μ-pz)$_6$] (pz=Pyrazolate) Showing Valence-Detrapping Behavior in Solution. *Chem. Eur. J.* **2006**, *12*, 6521–6727. [CrossRef]
19. Horiuchi, S.; Umakoshi, K. Recent advances in pyrazolato-bridged homo- and heterometallic polynuclear platinum and palladium complexes. *Coord. Chem. Rev.* **2023**, *476*, 214924. [CrossRef]
20. Baran, P.; Marrero, C.M.; Pérez, S.; Raptis, R.G. Stepwise, ring-closure synthesis and characterization of a homoleptic palladium(ii)-pyrazolato cyclic trimer. *Chem. Commun.* **2002**, *9*, 1012–1013. [CrossRef]
21. Mohamed, A.A. Advances in the coordination chemistry of nitrogen ligand complexes of coinage metals. *Coord. Chem. Rev.* **2010**, *254*, 1918–1947. [CrossRef]
22. Yu, S.-Y.; Lu, H.-L. From Metal-Metal Bonding to Supra-Metal-Metal Bonding Directed Self-Assembly: Supramolecular Architectures of Group 10 and 11 Metals with Ligands from Mono- to Poly-Pyrazoles. *Isr. J. Chem.* **2019**, *59*, 166–183. [CrossRef]
23. Galassi, R.; Rawashdeh-Omary, M.A.; Dias, H.V.R.; Omary, M.A. Homoleptic Cyclic Trinuclear d^{10} Complexes: From Self-Association via Metallophilic and Excimeric Bonding to the Breakage Thereof via Oxidative Addition, Dative Bonding, Quadrupolar, and Heterometal Bonding Interactions. *Comm. Inorg. Chem.* **2019**, *39*, 287–348. [CrossRef]
24. Canty, A.J.; Honeyman, C.T. Cyclometallation of polydentate ligands containing pyrazole groups, including the synthesis of platinum(IV) complexes with tripodal [NˆCˆN]- ligand systems. *J. Organomet. Chem.* **1990**, *387*, 247–263. [CrossRef]
25. Albrecht, M. Cyclometalation Using d-Block Transition Metals: Fundamental Aspects and Recent Trends. *Chem. Rev.* **2010**, *110*, 576–623. [CrossRef] [PubMed]
26. Cuesta, L.; Urriolabeitia, E.P. Cyclometallation of Heterocycles: A Reliable Strategy for Selective Functionalization. *Comm. Inorg. Chem.* **2012**, *33*, 55–85. [CrossRef]
27. Lu, W.; Mi, B.-X.; Chan, M.C.W.; Hui, Z.; Che, C.-M.; Zhu, N.; Lee, S.-T. Light-Emitting Tridentate Cyclometalated Platinum(II) Complexes Containing ó-Alkynyl Auxiliaries: Tuning of Photo- and Electrophosphorescence. *J. Am. Chem. Soc.* **2004**, *126*, 4958–4971. [CrossRef]
28. Koo, C.K.; Ho, Y.M.; Chow, C.-F.; Lam, M.H.-W.; Lau, T.-C.; Wong, W.-Y. Synthesis and Spectroscopic Studies of Cyclometalated Pt(II) Complexes Containing a Functionalized Cyclometalating Ligand, 2-Phenyl-6-(1H-pyrazol-3-yl)-pyridine. *Inorg. Chem.* **2007**, *46*, 3606–3612. [CrossRef]
29. Bossi, A.; Rausch, A.F.; Leitl, M.J.; Czerwieniec, R.; Whited, M.T.; Djurovich, P.I.; Yersin, H.; Thompson, M.E. Photophysical Properties of Cyclometalated Pt(II) Complexes: Counterintuitive Blue Shift in Emission with an Expanded Ligand π System. *Inorg. Chem.* **2013**, *52*, 12403–12415. [CrossRef]

30. Hashiguchi, B.G.; Bischof, S.M.; Konnick, M.M.; Periana, R.A. Designing Catalysts for Functionalization of Unactivated C-H Bonds Based on the CH Activation Reaction. *Acc. Chem. Res.* **2012**, *45*, 885–898. [CrossRef]
31. Lersch, M.; Tilset, M. Mechanistic Aspects of C-H Activation by Pt Complexes. *Chem. Rev.* **2005**, *105*, 2471–2526. [CrossRef]
32. Burger, W.; Strähle, J.Z. Pyrazolate and tetrazolate as bridging ligands in $[Pt(pz)_2]_3$, $[Pt(pz)_2]\infty$, and $[Pt(tz)_2]\infty$. Crystal structure of $[Pt(pz)_2]_3$. *Anorg. Allg. Chem.* **1985**, *529*, 111–117. [CrossRef]
33. Umakoshi, K.; Yamauchi, Y.; Nakamiya, K.; Yamasaki, M.; Kawano, H.; Onishi, M. Pyrazolato-Bridged Polynuclear Palladium and Platinum Complexes: Synthesis, Structure, and Reactivity. *Inorg. Chem.* **2003**, *42*, 3907–3916. [CrossRef]
34. Shannon, R.D. Revised effective ionic radii and systematic studies of interatomic distances in halides and chalcogenides. *Acta Crystallogr. A* **1976**, *32*, 751–767. [CrossRef]
35. Ma, B.; Li, J.; Djurovich, P.I.; Yousufuddin, M.; Bau, R.; Thompson, M.E. Synthetic Control of Pt···Pt Separation and Photophysics of Binuclear Platinum Complexes. *J. Am. Chem. Soc.* **2005**, *127*, 28–29. [CrossRef] [PubMed]
36. Baxter, L.M.A.; Heath, G.A.; Raptis, R.G.; Willis, A.C. Synthesis and Characterization of a Diplatinum(III)-Tetrakis(α-dioximato) Complex Containing an Unsupported Metal-Metal Bond. *J. Am. Chem. Soc.* **1992**, *114*, 6944–6946. [CrossRef]
37. Cini, R.; Fanizzi, F.P.; Natile, G. Synthesis and x-ray structural characterization of the first unbridged diplatinum(III) compound: Bis[bis(1-imino-1-hydroxy-2,2-dimethylpropane)trichloroplatinum(III)]. *J. Am. Chem. Soc.* **1991**, *113*, 7805–7806. [CrossRef]
38. Tadashi, Y.; Osamu, K.; Tasuku, I. An Unbridged Platinum(III) Dimer with Added Chloro Ligands in Equatorial Sites, $[Pt_2Cl_2(phpy)_4]$ (Hphpy = phenylpyridine), Synthesized by an Oxidation with Aurous Complex. *Chem. Lett.* **2004**, *33*, 190–191.
39. Lippert, B. Impact of Cisplatin on the recent development of Pt coordination chemistry: A case study. *Coord. Chem. Rev.* **1999**, *182*, 263–295. [CrossRef]
40. Vedernikov, A.N. Trivalent and Tetravalent Palladium and Platinum Organometallic Complexes. In *Comprehensive Organimetallic Chemistry IV*; Elsevier: Amsterdam, The Netherlands, 2021; pp. 1–53.
41. Ramanchenko, A.; Likhatski, M.; Mikhlin, Y. X-ray Photoelectron Spectroscopy (XPS) Study of the Products Formed on Sulfide Minerals Upon the Interaction with Aqueous Platinum (IV Chloride Complexes). *Minerals* **2018**, *8*, 578. [CrossRef]
42. Papadia, P.; Micoli, K.; Barbanente, A.; Ditaranto, N.; Hoeschele, J.D.; Natile, G.; Marzano, C.; Gandin, V.; Margiotta, N. Platinum(IV) Complexes of trans-1,2 diamino-4-cyclohexene: Prodrugs A_ording an Oxaliplatin Analogue that Overcomes Cancer Resistance. *Inter. J. Mol. Sci.* **2020**, *21*, 2325. [CrossRef]
43. Bader, R.F.W. *Atoms in Molecules: A Quantum Theory*; Oxford University Press: Oxford, UK, 1990.
44. Popelier, P.L.A. *Atoms in Molecules: An Introduction*; Prentice Hall: Upple Saddle River, NJ, USA, 2000.
45. Matta, C.F.; Boyd, R.J. (Eds.) *The Quantum Theory of Atoms in Molecules*; Wiley-VCH: Weinheim, Germany, 2007.
46. Perrin, D.D.; Armarego, W.L.F. *Purification of Laboratory Chemicals*, 2nd ed.; Pergamon Press: New York, NY, USA, 1987.
47. Data Collection: SMART-NT Software Reference Manual, version 5.0. ed. Bruker AXS, Inc.: Madison, WI, USA, 1998.
48. Data Reduction: SAINT-NT Software Reference Manual, version 4.0. ed. Bruker AXS, Inc.: Madison, WI, USA, 1996.
49. Sheldrick, G.M. A short history of SHELX. *Acta Crystallogr.* **2008**, *A64*, 112–122. [CrossRef] [PubMed]
50. Frisch, M.J.; Trucks, G.W.; Schlegel, H.B.; Scuseria, G.E.; Robb, M.A.; Cheeseman, J.R.; Scalmani, G.; Barone, V.; Mennucci, B.; Petersson, G.A.; et al. *Gaussian 09*; Gaussian, Inc.: Wallingford, CT, USA, 2009.
51. Becke, A.D. Density-functional exchange-energy approximation with correct asymptotic behavior. *Phys. Rev. A* **1988**, *38*, 3098–3100. [CrossRef] [PubMed]
52. Perdew, J.P. Density-functional approximation for the correlation energy of the inhomogeneous electron gas. *Phys. Rev. B* **1986**, *33*, 8822–8824. [CrossRef] [PubMed]
53. Reed, A.E.; Curtiss, L.A.; Weinhold, F. Intermolecular interactions from a natural bond orbital, donor-acceptor viewpoint. *Chem. Rev.* **1988**, *88*, 899–926. [CrossRef]
54. de Berrêdo, R.C.; Jorge, F.E. All-electron double zeta basis sets for platinum: Estimating scalar relativistic effects on platinum (II) anticancer drugs. *J. Mol. Struc. (Theochem)* **2010**, *961*, 107–112. [CrossRef]
55. Biegler-König, F. *AIM2000, Version 1.0*; University of Applied Sciences: Bielefeld, Germany, 2000.
56. Horiuchi, S.; Moon, S.; Ito, A.; Tessarolo, J.; Sakuda, E.; Arikawa, Y.; Clever, G.H.; Umakoshi, K. Multinuclear Ag Clusters Sandwiched by Pt Complex Units: Fluxional Behavior and Chiral-at-Cluster Photoluminescence. *Angew. Chem. Int. Ed.* **2021**, *60*, 10654–10660. [CrossRef]
57. Horiuchi, S.; Yang, Y.; Ueda, M.; Sakuda, E.; Arikawa, Y.; Umakoshi, K. Rational Synthesis of an Unsymmetric Pt Complex Unit Having Two Kinds of Pyrazolate Ligands, Elucidating Steric and Electronic Effects of Pyrazolate Ligands in Pt-Ag Sandwich Complexes. *Eur. J. Inorg. Chem.* **2022**, *2022*, e202200497. [CrossRef]
58. Roy, S.; Lopez, A.A.; Yarnell, J.E.; Castellano, F.N. Metal−Metal-to-Ligand Charge Transfer in Pt(II) Dimers Bridged by Pyridyl and Quinoline Thiols. *Inorg. Chem.* **2022**, *61*, 121–130. [CrossRef]
59. Park, H.J.; Boelke, C.L.; Cheong, P.H.-Y.; Hwang, D.-H. Dinuclear Pt(II) Complexes with Red and NIR Emission Governed by Ligand Control of the Intramolecular Pt−Pt Distance. *Inorg. Chem.* **2022**, *61*, 5178–5183. [CrossRef]
60. Xue, M.; Lam, T.-L.; Cheng, G.; Liu, W.; Low, K.-H.; Du, L.; Xu, S.; Hung, F.-F.; Phillips, D.L.; Che, C.-M. Exceedingly Stable Luminescent Dinuclear Pt(II) Complexes with Ditopic Formamidinate Bridging Ligands for High-Performance Red and Deep-Red OLEDs with LT97 up to 2446 h at 1000 cd m^{-2}. *Adv. Optical Mater.* **2022**, *10*, 2200741. [CrossRef]

61. Lai, S.-W.; Chan, M.C.W.; Cheung, K.-K.; Peng, S.-M.; Che, C.-M. Synthesis of Organoplatinum Oligomers by Employing N-Donor Bridges with Predesigned Geometry: Structural and Photophysical Properties of Luminescent Cyclometalated Platinum(II) Macrocycles. *Organometallics* **1999**, *18*, 3991–3997. [CrossRef]
62. Brown-Xu, S.E.; Kelley, M.S.; Fransted, K.A.; Chakraborty, A.; Schatz, G.C.; Castellano, F.N.; Chen, L.X. Tunable Excited-State Properties and Dynamics as a Function of Pt-Pt Distance in Pyrazolate-Bridged Pt(II) Dimers. *J. Phys. Chem. A* **2016**, *120*, 543–550. [CrossRef] [PubMed]
63. Chakraborty, A.; Deaton, J.C.; Haefele, A.; Castellano, F.N. Charge-Transfer and Ligand-Localized Photophysics in Luminescent Cyclometalated Pyrazolate-Bridged Dinuclear Platinum(II) Complexes. *Organometallics* **2013**, *32*, 3819–3829. [CrossRef]